Lawrence Berkeley National Laboratory

Title

In Situ Structural Observation of a Substrate- and Peroxide-Bound High-Spin Ferric-Hydroperoxo Intermediate in the P450 Enzyme CYP121

Permalink

https://escholarship.org/uc/item/1zp01492

Journal

Journal of the American Chemical Society, 145(46)

ISSN

0002-7863

Authors

Nguyen, Romie C
Davis, Ian
Dasgupta, Medhanjali
et al.

Publication Date

2023-11-22

DOI

10.1021/jacs.3c04991

Copyright Information

Peer reviewed

In situ structural observation of a substrate- and peroxide-bound high-spin ferric-hydroperoxo intermediate in P450 enzyme CYP121

Romie C. Nguyen,[1] Ian Davis,[1] Medhanjali Dasgupta,[2] Yifan Wang,[1†] Philipp S. Simon,[2‡] Agata Butryn,[3,4] Hiroki Makita,[2] Isabel Bogacz,[2] Kednerlin Dornevil,[1‡] Pierre Aller,[3,4] Asmit Bhowmick,[2] Ruchira Chatterjee,[2] In-Sik Kim,[2] Tiankun Zhou,[3,4] Derek Mendez,[2] Daniel Paley,[2] Franklin Fuller,[5] Roberto Alonso-Mori,[5] Alexander Batyuk,[5] Nicholas K. Sauter,[2] Aaron S. Brewster,[2] Allen M. Orville,[3,4] Vittal K. Yachandra,[2] Junko Yano,[2] Jan F. Kern,[2,*] and Aimin Liu[1,*]

[1]Department of Chemistry, University of Texas, San Antonio, TX 78249, United States

[2]Molecular Biophysics and Integrated Bioimaging Division, Lawrence Berkeley National Laboratory, Berkeley, CA 94720, United States

[3]Diamond Light Source, Harwell Science and Innovation Campus, Didcot, Oxfordshire OX11 0DE, United Kingdom

[4]Research Complex at Harwell, Rutherford Appleton Laboratory, Didcot, Oxfordshire OX11 0FA, United Kingdom

[5]LCLS, SLAC National Accelerator Laboratory, Menlo Park, CA 94025, United States

*Corresponding authors: Aimin Liu and Jan F. Kern

ABSTRACT: The P450 enzyme CYP121 from *Mycobacterium tuberculosis* catalyzes a C-C bond coupling cyclization of the di-tyrosine substrate containing a diketopiperazine ring, cyclo(L-Tyrosine-L-Tyrosine) (cYY). An unusual high-spin ($S = 5/2$) ferric intermediate maximizes its population in less than 5 ms in the rapid freeze-quenching study of CYP121 during the shunt reaction with hydrogen peroxide in acetic acid solution. We show that this intermediate is also observable in the crystalline state by EPR spectroscopy. By developing an on-demand-rapid-mixing method for time-resolved serial femtosecond crystallography with X-ray free-electron laser (tr-SFX-XFEL) technology covering the millisecond time domain, we structurally monitored the CYP121 reaction *in situ* at room temperature. After a 200-milliseconds peracetic acid-containing hydrogen peroxide reaction with the enzyme-substrate microcrystal slurry at room temperature, a ferric-hydroperoxo intermediate is observed. Its SFX crystal structure is determined at 1.85 Å resolution. The intermediate SFX structure has a hydroperoxyl ligand between the heme and the native substrate, cYY. The oxygen atoms of the hydroperoxo are 2.5 and 3.3 Å from the iron ion. The end-on binding ligand adopts a near-side-on geometry and is weakly associated with the iron ion, causing the unusual high-spin state for a compound 0-type of intermediate. The near side-on geometry and positioning of the hydroperoxo only 2.9 Å from the cYY phenol oxygen imply an active oxidant role of the intermediate for direct substrate oxidation in the non-hydroxylation carbon-carbon (C-C) bond coupling chemistry.

INTRODUCTION

The heme prosthetic group is ubiquitous, where its inimitable electronic properties are utilized by nearly every aerobic organism to catalyze a wide array of chemical reactions. Heme-based enzymes such as catalase, oxygenase, peroxidase, and peroxygenase share catalytic intermediates in the early stage of their reactions, which then deviate with distinct outcomes.[1] These intermediates can be short-lived, high-energy complexes, making their

characterization a challenge. A ferric-bound hydroperoxo intermediate, often termed compound 0 (cpd 0), is a common reaction intermediate of diverse heme enzymes.[2] Cpd 0 is a precursor for the iron(IV)-oxo porphyrin π-radical cation intermediate (compound I, cpd I),[3] a common active oxidant in heme-based chemistries (Scheme 1A). In some cases, the ferric-hydroperoxo intermediate can be used as an alternate oxidant instead of cpd I, such as in the proposed catalytic cycle of nitric oxide synthase and some engineered cytochrome P450 enzymes (CYPs).[4-6]

Cpd 0 is typically generated for characterization via cryoradiolytic reduction of the oxy-ferrous heme complex,[2, 5, 7-13] resulting in a ferric-peroxy anion intermediate which is readily protonated to ferric-hydroperoxo by a proton delivery network in systems such as myoglobin, peroxidases, and catalase.[1] Due to its reactive nature and typical lifetime of milliseconds (ms) or less, structural characterization of cpd 0 has been elusive from intermediates trapped during catalysis. Only very recently has a cpd 0 crystal structure captured during catalysis been obtained in the histidine-ligated heme-based tyrosine hydroxylase with an alternate fluorinated substrate[14] and lactoperoxidase with iodide in the active site.[15] In the P450 catalytic cycle, the dioxygen of cpd 0 has been proposed to bind in an end-on mode,[4] which is supported by experimental and theoretical evidence.[5] All reported ferric-oxo/hydroperoxo intermediates in heme-based biological systems are thus far situated with the oxygen species ligated to the heme iron in the end-on orientation, resulting in a 6-coordinate low-spin heme complex.

CYP121 is a cyrochrome P450 enzyme from *Mycobacterium tuberculosis* that catalyzes the formation of mycocyclosin through a two-electron and O_2-dependent reaction via the intramolecular C-C coupling between the tyrosyl moieties of cyclo(L-Tyrosine-L-Tyrosine) (cYY) (Scheme 1B).[16] This enzyme is essential for the viability of *Mycobacterium tuberculosis*,[17] making it a potential drug target.[18] Its reaction has an unusual characteristic at the first step of the catalytic cycle,[19] where substrate binding does not trigger a full spin-transition of the heme from low- to high-spin, as is typically observed in most P450 enzymes (Scheme 1). The low- to high-spin state transition can be initiated with the binding of a synthetic probe, cYY(O)Me, where CYP121 shows its true color as a P450 hydroxylase.[20] The enzyme-substrate (ES) complex of CYP121-cYY remains primarily low-spin, with a minor portion of high-spin observed at $g = 8.00$, 3.50, and 1.70 (Figure 1A, trace I), indicating a partial spin conversion. An X-band ENDOR study has shown that the lack of a clean spin transition is due to an equilibrium between no distal ligand, hydroxide, and aqua ligands.[21] The reaction catalyzed by CYP121 can also produce mycocyclosin through a catalytic shunt using hydrogen peroxide or peracetic acid (PAA). This organic peroxide is known to contain a percentage of hydrogen peroxide in solution due to manufacturing methods.[22] Transient kinetic studies using stopped-flow UV-vis and rapid freeze-quench EPR (RFQ-EPR) to observe the reaction of CYP121 with cYY and PAA show no spectroscopic sign of cpd I accumulation in CYP121 but rather, an unusual high-spin intermediate is observed after peracetic acid addition prior to the product formation.[19] A nearly complete conversion of the ES complex to the high-spin ferric heme-based intermediate has previously been observed, which formed in solution in the dead time after reacting the ES complex with PAA. The rapidly formed high-spin ($S = 5/2$) ferric intermediate was observed by RFQ-EPR with partial rhombicity and observed g-values of 6.87, 5.77, and 2.00 (Figure 1A, II).

The formation of this CYP121 intermediate requires both cYY and peracetic acid. It should be noted that the immediate and complete conversion of an ES complex to a high-spin ferric heme-based cpd 0 intermediate upon peroxide oxidation in CYP121 is the first example of its kind and unprecedented in heme chemistry. It is also

Scheme 1. Typical catalytic shunt pathway in cytochromes P450, including CYP121 with a substrate analog cYY(O)Me (A); and proposed catalytic pathway for CYP121 with its native substrate (B). The brackets denote proposed intermediates.
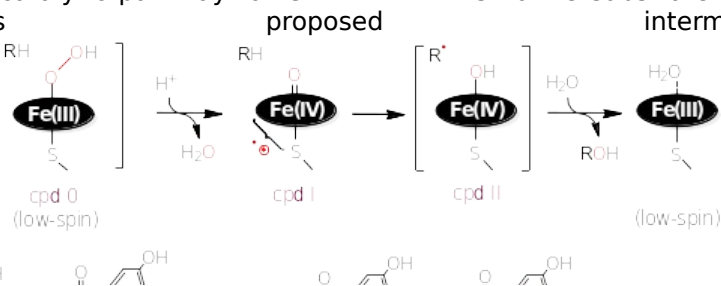
markedly different from low-spin to high-spin transitions induced by substrate-binding observed in many P450 and other heme enzymes prior to the addition of an oxidant (Scheme 1A), including the high-spin signal in CYP121 induced by binding of substrate analog cYY(O)Me,[20, 23] and is not generated by excess hydrogen peroxide at a pH range of 5 – 9. In the millisecond time domain, the unique high-spin ferric intermediate decays to an EPR-silent species. Until now, the chemical nature of the high-spin ferric heme-based intermediate remains uncharacterized Here, we report a unique high-spin ferric-hydroperoxo intermediate bridging the iron atom and substrate in a thiolate-ligated P450 enzyme characterized by time-resolved serial femtosecond crystallography, stopped-flow absorbance spectroscopy, and EPR.

In the present work, a slurry of single-crystals used in EPR spectroscopy has determined a sequential population of two distinct high-spin intermediates that have not been observed in P450 chemistry. The high-spin intermediate has only been observed to populate *in crystallo*, due to the highly transient nature in solution, and maximizes within 120 s to the rhombic high-spin species which has

been observed in solution state RFQ-EPR within a 5 ms dead time window of the mixing between the ES complex and peroxide. In an effort to structurally characterize this *in crystallo* observed intermediate by EPR, we utilized a Drop-on-Tape single-crystal rapid mixing method with PAA *vide infra*, in conjunction with *in situ*, time-resolved serial femtosecond crystallography (tr-SFX) with X-ray free-electron laser (XFEL) pulses.[24-25] With the development of the rapid-mixing method, we are able to observe directly, and in real time, the 5-ms high-spin ferric intermediate at room temperature without quenching. Together with single-crystal slurry EPR spectroscopy, we describe an unprecedented thiolate-ligated heme intermediate structure which suggests that CYP121 utilizes cpd 0 and iron(IV)-oxo (compound II, abbreviated as cpd II) to oxidize its cYY substrate for C-C coupling. This mechanism is distinct from the well-characterized pathway of hydroxylating P450s.

EXPERIMENTAL PROCEDURES

Protein expression and purification. The methods for growth and expression of CYP121 from *Mycobacterium tuberculosis* in *Escherichia coli* strain BL21(DE3) and purification have been previously described.[19] The isolated enzyme is known to be a functional homodimer with a buried surface area of 1300 $Å^2$ based on the recent ^{19}F NMR studies,[26-28] though it crystallizes as a monomer. The enzyme purity was judged based on SDS-PAGE electrophoresis and R_Z values, and the activity assay was described previously.[19-20] Peracetic acid was purchased from Sigma-Aldrich, which contained 39% peracetic acid and 6% hydrogen peroxide (13% of the total peroxide).

Preparation of crystal complexes. Before crystallization, the *N*-terminal His$_6$-tag was cleaved from CYP121 and cocrystallized with cYY using the procedure described previously.[20-21] Crystals were obtained from drops with a 1:1 ratio of the pre-formed ES complex (10 – 14 mg/mL enzyme in 50 mM Tris-HCl pH 7.4, 2 mM cYY) to mother liquor solution after a growth period of 2 – 4 weeks. Figure S1 shows the packing in the crystal lattice.

Stopped-flow absorption spectroscopy. Stopped-flow studies were carried out on an Applied Photophysics SX20 stopped-flow system using a

photodiode array to obtain multi-wavelength kinetic data. The assay conditions consisted of 5 μM CYP121, 400 μM cYY, and 0.25 – 32 mM hydrogen peroxide after rapid mixing. A stock solution of 76 mM cYY was made by dissolving the substrate in DMSO, keeping the DMSO concentration less than 2% (v/v) after mixing. To mitigate enzyme degradation from addition of concentrated amounts of DMSO, the substrate was suspended in buffer before addition of enzyme. Experiments were carried out at 22°C in 100 mM potassium phosphate buffer at pH 5, 7.4, and 9.

Rapid freeze-quench EPR spectroscopy.
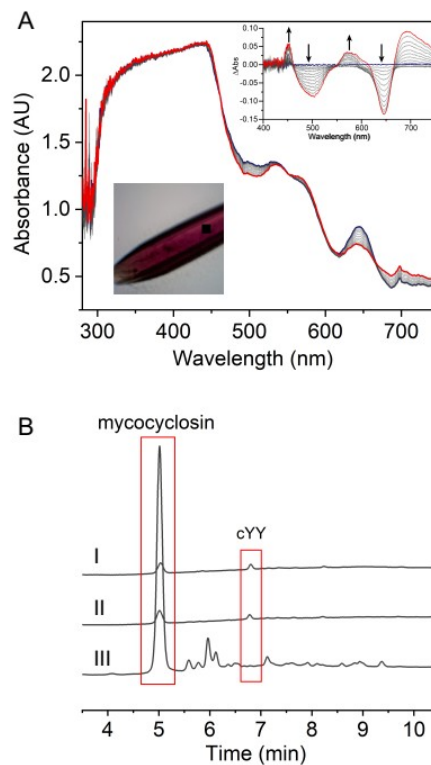
Figure 2. Single-crystal UV-vis monitoring of the CYP121 ES complex crystal reaction with peracetic acid and crystal reaction product analysis. **(A)** ES complex reaction with peracetic acid monitored by a single-crystal UV-visible microspectrophotometer in real-time. An image of the crystal and the difference spectra is shown in the inset. The initial ES complex spectrum (navy) is observed to transition to the E only state (red) by the shifting of the α/β band and decay of the charge transfer band, which indicates loss of the ligand from the active site. This ES to E transition is observed in the minutes time window depending on the size of the single-crystal, and it suggests substrate-to-product conversion. **(B)** HPLC analysis of the supernatant from CYP121-cYY crystal reaction with peracetic acid. (I) Mother liquor in which crystals are stored in. (II) mother liquor with 2 mM peracetic acid.

Experiments were carried out using a System 1000 chemical/freeze-quench apparatus made by Update Instruments, Inc. An isopentane bath was maintained at −155 °C and liquid ethane used to rapidly freeze the ejected sample and filled the EPR tube during sample packing. Reactions were carried out by mixing 409 μm CYP121 and 1 mM cYY with 20 mM PAA in a 1:1 ratio at room temperature in buffer consisting of 50 mM Tris-HCl, pH 7.4. The reaction
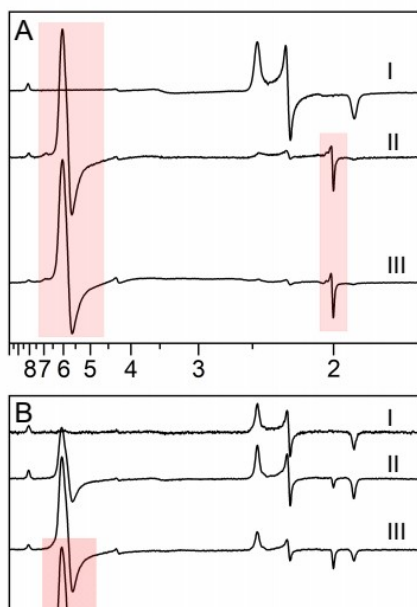
into a 4 mm quartz EPR tube containing mother liquor for a final volume of 200 μL. Crystals were evenly dispersed throughout the sample before rapidly freezing in liquid ethane to measure the ES complex. Parallel samples were made, and peracetic acid was added to a final concentration of 5 mM, rapidly manually mixed, and frozen for each time point. EPR spectra were recorded at 9.4-GHz microwave frequency with 1.002 mW power using a Bruker E560 EPR spectrometer with an SHQE-W resonator at 100-kHz modulation frequency and 0.6 mT modulation amplitude. The temperature was maintained at 20 K by a cryogen-free 4K temperature system. Quantitative simulation of the EPR spectra was performed with EasySpin,[29] and the simulation parameters are given in Table S1.

Product analysis. Crystals previously harvested and stored were used for reaction with peracetic acid. An aliquot of crystals was placed in a new 1.5 mL Eppendorf tube after resuspending the crystals in the storage tube. The crystals were pelleted, and crystallization buffer removed and set aside for use as control samples leaving approximately 10 μL crystal volume. The control sample was partitioned into two tubes with one charged with peracetic acid to a final concentration of 2 mM. A fresh 2 mM peracetic acid solution was prepared in crystallization buffer and used to resuspend the crystals. The reaction was stopped after 1 hr by pelleting the crystals and removing the supernatant, which was then filtered with a 10 Kda centrifugal filter (Millipore) before 20 μL of filtrate was loaded onto an InertSustain C18 column (5μm particle size, 4.6 X 100 mm, GL Sciences Inc.). The samples were analyzed using a Thermo Scientific Ultimate-3000SD HPLC rapid separation system equipped with a photodiode array detector. The chromatograms were recorded with a full range of wavelengths from 190 to 800 nm and HPLC profiles presented in this study were chromatograms monitored at 295 nm. The elution method has been previously described.[19]

SFX and Structural determination of the ES complex crystals and the reaction with PAA. SFX-XFEL diffraction data presented in this work were collected at the Linear Coherent Light Source (LCLS), Menlo Park, CA, during experiments LU50, LV43, P112, and P199A. The ES complex crystals were vortexed using a Teflon bead (Hampton Research Inc) to reduce their size to ~30 μm in a 1.5 mL Eppendorf tube and the appropriate mother liquor. Vortexing causes the crystals to crack in the x, y, and z axes, greatly reducing their size and increasing their surface area. The resulting microcrystal slurry was measured for the resting state or mixed with peracetic acid directly before X-ray exposure using the drop-on-drop approach described recently and updated in the main text. In this setup, the crystal slurry was dispensed onto a Kapton conveyor belt in the form of 2 nL droplets at 30 Hz deposition frequency using an acoustic injector[24] resulting in a sample consumption rate of 3.6 μL/min. A second droplet dispenser located 40 mm upstream of the X-ray interaction point was used to dispense a burst of 10 droplets of 60 pL each of a 250 mM stock solution of peracetic at a rate of 1.6 kHz onto the same conveyor belt.[25] Droplet ejection was triggered in such a way that two droplets out of each burst hit and mixed with each of the larger crystal slurry drops resulting in a final concentration of 14 mM peracetic acid in the crystal-containing drop. The drops were transported at a belt speed of 200 mm/s from the droplet mixing to the X-ray interaction point, resulting in a delay between mixing and X-ray probing of 200 ms. Diffraction data were collected at 1.30 Å wavelength using a Rayonix MX340-HS detector in 4x4 binning mode at a repetition rate of 30 Hz with 4 mJ/pulse (LU50) or 2.2 mJ/pulse (LV43), a pulse duration of ~35 fs, and an X-ray beam size at the sample of ~3 μm in diameter.

Data acquisition was tracked with the *cctbx.xfel* graphical user interface.[30] The jobs run the core program *dials.stills_process* to index and integrate the images while providing real-time feedback, as part of the larger *cctbx.xfel* and DIALS processing suite.[31-35] A first estimate of the detector position (distance and beam center) was obtained from a powder diffraction pattern of silver(I) behenate (Alfa Aesar). After initial spot finding, followed by indexing strong reflections and integration using *dials.stills_process*, a round of metrology refinement was done. The second round of indexing and integration was performed with the refined detector position. After correction of the integrated intensities for absorption by the Kapton conveyor belt, final data integration and merging were performed using *cctbx.xfel.merge* using the ev11 error model with the synchrotron structure (5WP2.pdb) as reference. The small molecules used for modeling (YTT, HEM, and PEO for cYY, heme, and hydroperoxo) were fetched from the PDB, and Phenix generated the ligand restraints. Justification of the resolution cut-off for the merged data was determined based on multiplicity in the highest resolution shell and on $CC_{1/2}$ (monotonic decrease).

Data refinement was completed using Phenix.[36] The small molecule parameter files were downloaded from the PDB and refined into the structure one at a time. The R_{free} test sets for each data set utilized the default setting in phenix.refine (10%) and phenix was allowed to optimize this

during refinement. To determine occupancy level of the hydrogen peroxide heme ligand, the oxygen atoms of the ligand were analyzed in a stepwise reduction fashion from 0.90 – 0.30 and refined at each step with the occupancies box unchecked in the refinement strategy. When the dictated occupancy level showed no overfitting or underfitting of the ligand model, the occupancies box was checked under refinement strategy to allow phenix to optimize the occupancy level of the ligand.

RESULTS

Observation of the high-spin intermediate by single-crystal slurry EPR spectroscopy. The production phase of the high-spin ferric heme-based intermediate after peroxide addition to the ES complex is before the deadtime of the freeze quench setup in the solution state. Therefore, we attempted to observe this intermediate in the crystalline state. The single-crystals of CYP121 in complex with its substrate, cYY, were obtained as described previously.[20-21] For EPR measurement of the ES complex, approximately one thousand equivalent co-crystalized single-crystals in a mother liquor solution were transferred in random orientation to an EPR tube, flash-cooled with liquid ethane, and stored in liquid nitrogen. The large number of crystals used was necessary for signal averaging due to varying crystal orientations in the sample tube. EPR analysis of the crystal slurry revealed an expected 6-coordinate, low-spin (LS) ferric heme species (g_z, g_y, g_x: 2.45, 2.24, 1.91), which matches the observed spectrum of the solution state ES complex (Figure 1A, I). A small percentage of rhombic heme species exists in the high-spin (HS) state with resonances observed at $g = 8.09$, 3.55, and a g_x value indiscernible from the baseline is present. It belongs to the ES complex, not the resting state (Figure 1A, I), as found previously.[19] Thus, the typical substrate-induced low- to high-spin transition for P450 enzymes is not observed in EPR with a slurry of crystals, consistent with the solution EPR results. The majority of the cYY-CYP121 complex remains in the LS state.

Four parallel samples, each containing thousands of the ES complex crystals, were used for reaction with peracetic acid and flash-cooled in liquid ethane in order to achieve time points in each of the replication experiments. The ms time domain is inaccessible for EPR characterization of *in crystallo* reaction using hand mixing, with the fastest access time being approximately 5 s for mixing, reaction, and freezing. Within 30 s of reaction, a new high-spin signal with observed g-values of 6.43, 5.76, and 2.00 appears in the spectrum (Figure 1B, III), which maximizes at 120 s. Formation of this signal is accompanied by near-complete disappearance of the initial ES complex high- and low-spin heme signals (Figure 1B, I). Comparison of the single-crystal slurry EPR spectra to solution-state RFQ-EPR shows that the 60 and 120 s spectra consistent with the 5 – 500 ms RFQ-EPR spectra shown in Figure 1A (spectra II and III in Figure S2. Simulation of the 120 s spectrum without a rhombic 6-coordinate high-spin component (Figure S3) led to residuals showing imperfect fitting, indicating that the $g = 6.43$ resonance is an integral component of
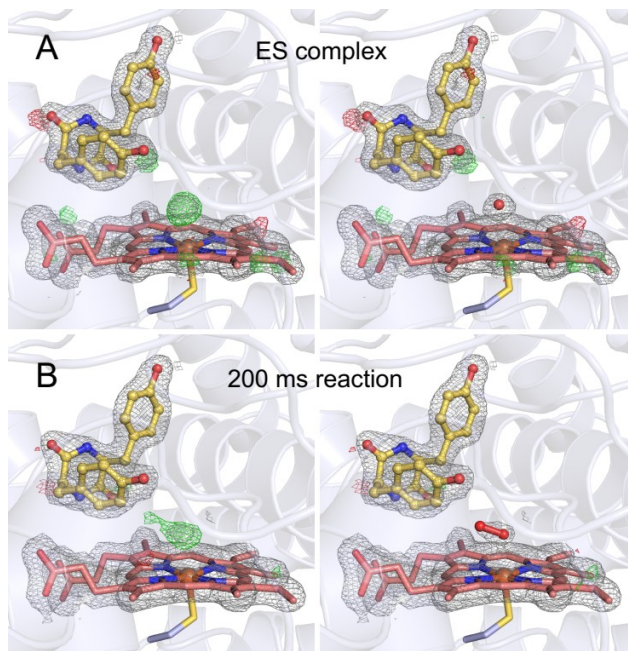
Figure 3. A hydroperoxyl ligand observed *in situ* by time-resolved SFX-XFEL of CYP121 cocrystallized with cYY microcrystal slurry reacted with peracetic acid for 200 ms. (A) The ES complex at 1.65 Å resolution (7S0O.pdb) and (B) the 200 ms intermediate at 1.85 Å resolution (7RUK.pdb). The $2F_o$-F_c electron density map is contoured at 1 σ (gray), and the F_o-F_c electron density map is contoured at 3 and -3 σ (colored green and red, respectively). The left panels show the omit map of the ES complex and the 200 ms intermediate without modeling the sixth ligand in the axial position of the heme iron. In contrast, the right panels show the electron density after modeling a ligand. For the 200 ms intermediate, the shape of the omit map is elongated rather than spherical, as expected for a

the spectrum (Figure S3). The minor g-value shift is due to the difference between the solution and crystalline states, as the $g = 8.09$ resonance of the ES complex was previously noticed at $g = 8.11$ in the solution state.[19] The relative concentrations of the EPR-active species and simulation parameters used for quantification can be found in Table S1, and each component used to reconstruct the entire 120 s single-crystal slurry EPR spectrum is found in Figure S4. The simulation shows five components: a low-spin, 5-coordinate high-spin, axial 6-coordinate

Table 1. Time-resolved room temperature SFX-XFEL data collection and refinement statistics for the ES complex and 200 ms reaction intermediate with peracetic acid.

| Description	CYP121 + cYY complex (ES)	Ternary complex (Cpd 0)
oxidant	no oxidant	Δt = 200 ms
PDB entry	7S0O	7RUK
data collection		
no. of lattices	10850	11569
used for refinement		
space group	P6$_5$22	P6$_5$22
a, b, c (Å)	78.6a, 78.6, 78.6	78.7a, 78.7
	205.2	265.9
α, β, γ	90, 90, 120	90, 90, 120
resolution	33.2 – 1.85	
	(1.68 – 1.65)a	(1.92 – 1.85)a
no. of unique reflections	58932	41826
redundancy	67.1 (9.8)	48.3 (1.8)
R_{split}	0.14 (1.042)	0.20 (0.92)
$I/\sigma I$	4.54 (0.538)	3.01 (0.587)
completeness	99.9 (99.7)	99.9 (98.9)
$CC_{1/2}$	0.984 (0.140)	0.84 (0.257)
Refinement		
resolution (Å)	31.8 – 1.65	33.2 – 1.85

high-spin, rhombic 6-coordinate high-spin, and isotropic $g = 4.27$ signal present in the spectrum.

Parallel-mode EPR detected no integer-spin signals from PAA oxidation of the crystal slurry. With the high concentration of PAA to maximize production of the 120 s high-spin intermediate, no regeneration of the initial low-spin species was noted during the decay of the intermediate high-spin signal. The similarity between the 120 s high-spin heme signal generated *in crystallo* and RFQ in solution supports the same intermediate formed in both states. To confirm the high-spin species detected by EPR are on-pathway and therefore catalytically relevant, one intact crystal was exposed to oxidant and monitored by UV-visible spectroscopy on the minutes time scale. It was observed to transition from the cYY-CYP121 complex to the ligand-free CYP121 via the α/β and charge transfer bands, indicative of product leaving the active site (Figure 2A). This was confirmed by a bulk *in crystallo* reaction where the supernatant analyzed by HPLC showed an elution at 5 min with the UV-visible spectrum correlating with previous reports of mycocyclosin (Figure 2B). Detection of mycocyclosin in conjunction with these *in crystallo* reactions monitored by EPR resemble solution state reaction RFQ-EPR spectra, which indicates that these observed intermediates are indeed on-pathway and, therefore mechanistically relevant.

Structural characterization of the early intermediate by time-resolved SFX-XFELs. To access early reaction intermediates during CYP121 turnover, we improved our recently developed drop-on-drop method for studying reactions *in crystallo*.[24-25] This approach utilizes the Drop-on-Tape approach but includes a second droplet dispenser that allows for the addition of tiny volume droplets to a large crystal slurry containing drops at variable delay times before X-ray probing. A photograph of this mixing device is shown in Figure S5. This on-demand strategy rapidly mixes and initiates reactions of almost any substrate over a wide range of concentrations within any microcrystal slurry to study catalytic reactions ranging from tens of ms to several seconds (see Methods for details). Substrate concentration, mixing, and reaction initiation are a function of how many ~30 – 80 pL volume droplets (between 0 – 50) are added with turbulent force to the approximately 2 – 4 nL crystal slurry drop as it moves toward the X-ray interaction region. Each particular reaction time point is determined by the speed of the Kapton belt and the distance between the droplet mixing point and the X-ray interaction region.[25] Compared to the previous version of the setup, we reduced the distance between the mixing point and the X-ray interaction region, enabling us to access shorter mixing times, and improved the control and visualization of the droplet collision region, allowing for the reproducible addition of a larger number of droplets to the microcrystal slurry drops. Since the SFX-XFEL method requires microcrystals, we conducted tr-SFX experiments with needle-like microcrystal slurries of the co-crystalized CYP121 ES complex, and each microcrystal within the slurry was approximately 30 μm in length or smaller. The unique high-spin intermediate formed in less than 5 ms in solution

and 120 s in large crystals is expected to develop in the millisecond time domain because the smaller the crystal, the faster the ligand diffusion, and hence, the reactions.[37-38] It should be noted that peracetic acid is not a pure solution due to manufacturing methods and thus consists of approximately 39% peracetic acid, 6% H_2O_2, and 55% acetic acid. We quantified the percentage of H_2O_2 present in the peracetic acid solution used in our experiments to be 5.5 ± 0.3 wt% by ceric sulfate titration using previously reported methods.[22]

The SFX-XFEL dataset of the ES complex (Figure 3A) was refined to 1.65 Å resolution (Table 1). The tr-SFX datasets were obtained from an ES microcrystal slurry in mother liquor to which we added 14 mM PAA (optimized for the tr-SFX-XFEL setup), which contains 1.8 mM H_2O_2. Reaction times ranged from 200 ms to seconds at room temperature before reaching the X-ray interaction region for diffraction. The tr-SFX crystal structure was solved by molecular replacement and refined to 1.85 Å resolution (Table 1). The atomic models for the 200 ms intermediate structure and the ES complex are very similar, with no significant identifiable electron density differences observed on the protein or the cYY substrate, but with apparent differences visible at the heme iron. Comparing the axial ligand electron density shape and ligand fittings of all tr-SFX data sets in hand from 200 ms to
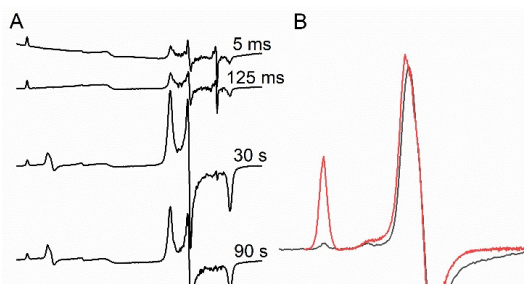
90 s (the latter obtained by in-well mixing rather than the drop-on-drop strategy), we found that the 200 ms tr-SFX electron density is fit most appropriately with an atomic model of a heme-bound hydroperoxo intermediate (cpd 0). This newly observed elongated electron density (Figure 3B) is not present in the ES complex or at longer reaction times at room temperature by tr-SFX.

~~Assignment of the partial hydroperoxo and partial water axial ligand stems from observations of the RFQ-EPR spin-state transition from the 5 ms time point and~~ An initial refinement of a water molecule into the ligand density of the 200 ms tr-SFX dataset

resulted in an incomplete fit with excess electron density observed adjacent to the water and appropriately sized for an oxygen atom (Figure S6, panel B). Attempts to fit peracetic acid into the axial ligand electron density at 100% and 50% occupancy resulted in unsatisfactory refinements (Figures S6 C & D). At full occupancy, the peroxide ligand is clearly over-fitted (Figure S7), whereas reducing occupancy to 52% yielded a satisfactory fit for all axial ligand electron density with no over- or under-fitted difference features present (Figure 3B).

Notably, this peroxide ligand is relatively weakly associated with the iron ion. The Fe-O1 and Fe-O2 distances are 2.43 ± 0.11 and 3.27 ± 0.19 Å, respectively, the O1-O2 bond length is 1.41 ± 0.10 Å, and the Fe-S(Cys345) bond length is 2.40 ± 0.03 Å (Figure S8). The accuracy of these positional assignments was determined by perturbation of the structure factors ($\pm[F_{obs}-F_{model}]$) of the model using the END RAPID method which allows the assignment of coordinate errors to individual atoms. The structure factors are randomly perturbed in the target model generating 100 trials,[39] followed by re-refinement of each of the perturbed datasets using Phenix, which generates standard deviations of the reported atom positions.

The observed Fe-O1 and Fe-O2 distances are greater than an expected Fe-O bond (average 2.15 Å length), indicating a weakly associated hydroperoxyl ligand in a five- or six-coordinate ferric heme center with a weak axial ligand, consistent with the high-spin state observed by EPR spectroscopy. The Fe-O1-O2 angle of 111.2° and a (Cys345)S-Fe-O1-O2 torsion angle of -162.2° further indicate that the peroxide ligand is situated in a near side-on orientation. Thus far, side-on binding has not been observed in any heme-based biological systems and was previously only characterized in several model complexes.[40-46] It should be noted that this ferric-hydroperoxo differs from those reported in porphyrin model complexes with a mixed N/O ligand set. To date, neither end-on nor side-on peroxo intermediates have been structurally observed in heme-dependent iron enzymes with an axial thiolate ligand through direct observation or trapping method. This ferric-hydroperoxo found in CYP121 with its native substrate is thus the first of its kind.

Rapid freeze-quench EPR reveals the protonation state of the observed structural intermediate from SFX. While the tr-SFX-XFELS structure study shows an unprecedented axial hydroperoxo heme ligand, the observed Fe-O1 bond length of 2.43 Å is significantly longer compared to the average of 1.8 Å for a heme Fe-O ligand reported in other low-spin heme Fe-O bound peroxo structures, but only slightly longer than the 2.3 Å average length observed for cpd 0 directly trapped in the reaction with a substrate (Table 2).[14-15] Reported Fe-O bond distances for non-porphyrin-based model complexes with a thiolate-aryl ligation

and *tert*-butyl-peroxide ligand are longer, ranging from 2.74 – 2.85 Å. Additionally, the observation of a hydroperoxo rather than a peracetate ligand when using an organic alkylperacid raises questions.

As mentioned earlier, the peracetic acid solution consists of acetic acid, peracetic acid, and H_2O_2 (55%, 39%, 5.5%, respectively) with corresponding pK_a values of 4.8, 8.2, and 11.8. Due to the multiple components present in solution, we interrogated the effect of each component on the formation of the heme axial ligand and defined that the high-spin species is generated specifically by peracetic acid and not H_2O_2 or acetic acid. Additionally, the effect of pH on cpd 0 formation using hydrogen peroxide was screened to ensure that the lack of observed high-spin species was not due to the protonation state. Firstly, with the high amount of acetic acid present in the oxidant solution, the effect of pH on formation of the high-spin signal was screened using hydrogen peroxide as the oxidant to determine its ability to initiate the low- to high-spin transition. A pH range of 5 – 9 was screened by RFQ of the ES complex reacting with hydrogen peroxide and measured by EPR to determine whether a high-spin signal similar to that observed when using peracetic acid would be generated (Figure S9). When monitoring the reaction within this pH range at progressive time points, the dominant species remained to be low-spin heme with a small fraction of high-spin heme present, indicating that hydrogen peroxide does not contribute to the high-spin heme intermediate despite the observation of the hydroperoxo ligand in the tr-SFX structure. Additionally, at high pH and long reaction time points, a minor equilibrium low-spin species is observed with *g*-values of 2.32, 2.17 (Figure S10). These *g*-values correspond to those ferric-hydroperoxo heme species from cytochromes P450 that have been artificially generated by cryoradiolytic reduction and characterized.

Next, a 10% hydrogen peroxide solution was made using glacial acetic acid to mimic the conditions of the peracetic acid solution, sans the peracetic acid, and aged for a minimum of 24 h at 4°C (Figure 4). The buffer capacity was increased to 250 mM to ensure the pH was within reason upon mixing a high oxidant concentration with the ES complex. At early time points, no low- to high-spin transition is observed. In the seconds time domain, a small fraction of low-spin heme transitions to the high-spin heme species. This signal was normalized to the ferric-hydroperoxo high-spin intermediate generated via peracetic acid in 5 ms and overlaps well, indicating that the same cpd 0 intermediate is formed in both cases (Figure 4B). The use of acetic acid alone does not generate the high-spin signal at any time point (Figure S11), demonstrating that only the hydrogen peroxide in acetic acid is able to form the cpd 0 intermediate, albeit less efficiently compared to peracetic acid.

Table 2. Reported Fe-O bond distances in structurally characterized enzyme and model ferric-peroxo complexes

Enzyme	Intermediate	Fe-O (Å)	O-O (Å)	Methodology	PDB entry	Ref.
CYP121 (ternary)	ferric-hydroperoxo	2.5	1.4	direct observation	7RUK	this

		Fe-O (Å)	O-O (Å)	Methodology	PDB	work [47]
CYP121 (binary)	ferrous-oxy	2.14	1.23	synchrotron radiation	1N40	[47]
tyrosine hydroxylase		2.2	1.4	directly trapped	7KQU	14
		2.4	1.4			
lactoperoxidase		2.41	1.48	directly trapped	7DN6	15
		2.33	1.49		7DN7	
chloroperoxidase	ferric-hydroperoxo	1.8	1.5	photoreduction	2J5M	2
myoglobin (sperm whale)	ferric-peroxo	1.85	1.33	synchrotron radiation	2Z6T	10
myoglobin (horse heart)	ferric-peroxo	1.84	1.34	cryoreduction	2VLX	11
	ferric-hydroperoxo	1.78	1.50			
oxy-F33Y-CuB-myglobin (sperm whale)	ferric-hydroperoxo	1.84	1.22	cryoreduction	5HAV	12
H128N catalase	ferric hydrogen peroxide complex	2.56	1.54	mutation, soaking	1GGF	[48]
		2.89	1.51			
		3.01	1.52			
		3.29	1.52			

Model complex	Compound	Fe-O (Å)	O-O (Å)	Methodology	Ref.
$[Fe^{III}([15]aneN_4)(SC_6H_5)(OO^tBu)]^+$	ferric-alkylperoxo	2.74	3.03	synthesized	[49]
$[Fe^{III}([15]aneN_4)(SC_6H_4\text{-}p\text{-}Cl)(OO^tBu)]^+$	ferric-alkylperoxo	2.75	3.03	synthesized	[49]
$[Fe^{III}([15]aneN_4)(SC_6H_4\text{-}p\text{-}OMe)(OO^tBu)]^+$	ferric-alkylperoxo	2.71	3.03	synthesized	[49]
$[Fe^{III}([15]aneN_4)(SC_6H_4\text{-}p\text{-}NO_2)(OO^tBu)]^+$	ferric-alkylperoxo	2.77	3.02	synthesized	[49]
$[Fe^{III}([15]aneN_4)(SC_6H_4\text{-}p\text{-}SC_6F_5)(OO^tBu)]^+$	ferric-alkylperoxo	2.85	3.01	synthesized	[49]

It is important to distinguish between two possibilities for the heme ligand represented by the high-spin signal observed in the *in crystallo* reactions, RFQ-EPR solutions state studies, and tr-SFX structure induced with PAA: (1) a very weakly associated, singly protonated peroxo ligand or (2) a fully protonated hydrogen peroxide adduct. As noted before, H_2O_2 is not as catalytically efficient as PAA in the CYP121-cYY reaction at pH 7.4 and 9, and higher H_2O_2 concentration is needed for substrate turnover.[19-20] Next, we revisited the pH dependence of the PAA-dependent reaction. Stopped-flow absorption spectroscopy was used to track the enzymatic reaction with hydrogen peroxide at pH 5, 7.4, and 9, which distinctly differs from the reaction kinetics of PAA (Figure S12). As previously characterized, upon addition of PAA, a transition from the ES complex to E is observed, with the decrease of the 395 nm band and concomitant increase at 427 nm within 300 ms, which redshifts over time to 433 nm.[19] The use of H_2O_2 resulted in stark differences from PAA where an initial decrease of the ES complex Soret band at 395 nm and an increase at 419 nm within 50 ms was observed with no obvious changes elsewhere on the spectrum (Figure S13). At 100 ms, this 419 nm band disappears, and the major shift turns to the decrease of the ES complex Soret up to 5 s with a band increasing at 441 nm through 60 s of the reaction. As the pH increases, this initial transition observed within 50 ms is much less pronounced. Over a period of 60 s, the enzyme-only Soret band expected at 419 nm never recovers, likely due to an equilibrium species from the high concentration of hydrogen peroxide used. The RFQ and hand-mixed EPR samples of ES complex reaction with H_2O_2 at pH 5 used to probe the heme center at progressive time points revealed a similar observation regarding spectral differences compared to peracetic acid (Figure S9A). As described above, no low- to high-spin transition of the heme is observed when using H_2O_2 alone as the oxidant. Rather, the initial transition within 30 ms results in a decrease of low-spin signal intensity coupled with the appearance of a minor radical signal at $g = 2.008$, which maximizes between 125 – 500 ms and then disappears in the seconds time domain. The decrease of the low-spin signal indicates formation of an EPR silent species, likely cpd II, and the signal is not fully re-formed until after 500 ms. The small percentage of high-spin signal observed in both the E and ES complex does not change throughout the reaction, indicating that it is an inactive form of the heme. These details are in stark contrast to the use of PAA as an oxidant where upon mixing with ES complex, a rhombic high-spin heme species in the *in-crystallo* reactions is detected. Thus, with the use of H_2O_2 and lack of formation of the PAA-induced high-spin ferric heme-based intermediate previously observed, the 200-ms structure represents a cpd 0 intermediate corresponding to the unique 6-coordinate rhombic high-spin heme observed in solution-state RFQ and single-crystal slurry EPR.

DISCUSSION
The cpd 0 heme intermediate in cytochromes P450 has been extremely challenging to capture due to its inability to accumulate before cpd I formation. Thus, the major technique that has been deployed to generate this intermediate is cryoradiolytic reduction of the oxy-ferrous P450 complex at low temperatures coupled with an annealing process at progressively higher temperatures to track the degradation of the ferric-hydroperoxo complex.[50] These trapped and characterized complexes of oxygen-inserting enzymes, P450cam,[51] P4502B4,[52] and P450ssc,[53] have the ferric-hydroperoxo as low-spin heme, consistent with a 6-coordinate end-on

hydroperoxo ligand (*g*-values summarized in Table 3). In sharp contrast, the observations described in this study indicate the presence of a high-spin cpd 0 intermediate (Scheme 1B), observed in solution and *crystallo* initiated by adding an oxidant and observed at room temperature.

Table 3. *g*-Values of ferric high-spin, low-spin, and hydroperoxo heme species in cytochromes P450 and other heme-dependent enzymes.

Enzyme	Method	Substrate	High-spin g_1, g_2, g_3		Low-spin g_1, g_2, g_3		Hydroperoxo g_1, g_2, g_3		ref	Chemistry
CYP121		none	8.10, 1.7	3.50,	2.49, 1.89	2.25,			19	C-C bond forming
CYP121		cYY[a]	8.11, 1.7	3.50,	2.45, 1.90	2.25,			19	
CYP121	oxidant	cYY+PAA[b]	8.09, n.d.	3.50,	2.45, 1.90	2.25,	6.87, 2.00	5.77,	19, this work	
CYP121	oxidant	cYY+H$_2$O$_2$	8.10, n.d.	3.50,	2.48, 1.90	2.25,	2.32, 2.17, nd		this work	
P450cam	cryoradiolytic reduction	camphor	8.0, 4.0, 1.8		2.41, 1.96	2.21,	2.29, 1.96	2.17,	[51, 54]	*O*-insertion
P4502B4	O$_2$-saturated buffer	Bnz[c]+CPR[d]	8.11, n.d.	3.55,	2.41, 1.92	2.23,	2.32, 1.95	2.16,	[52, 55]	*O*-insertion
P450ssc	cryoradiolytic reduction	none					2.34, 1.95 2.37, 1.95	2.18. 2.18,	[53, 56]	*O*-insertion
horseradish peroxidase	cryoradiolytic reduction	none					2.32, 1.94	2.18,	[57]	reduction
chloroperoxidase	cryoradiolytic reduction	none					2.28, 1.95	2.18,	[57]	halogenation

a, cYY, cyclo(L-tyrosine-L-tyrosine), *b*, PAA, peracetic acid, *c*, Bnz, benzphetamine, *d*, CPR, cytochrome P450 reductase, *n.d.*, not determined

Those reported ferric-hydroperoxo intermediates generated by cryoradiolytic reduction are representative of hydroxylating P450s, but do not necessarily include the less studied subset of P450s that perform other chemistries such as C-C and C-N bond forming/bond breaking reactions. Initiating the CYP121 C-C coupling reaction with peracetic acid yields a high-spin heme signal that has never been reported in thiolate-ligated heme systems and, to the best of our knowledge, is unique to the CYP121 ternary complex. Indeed, if a high concentration of H$_2$O$_2$ is mixed with enzyme and reacted for 40 s (*g* = 2.32, 2.17, n.d.), a minor ferric-hydroperoxo heme is observed that is consistent with those cryoradiolytically reduced cpd 0 intermediates. However, due to the long time point, this is likely an inactive equilibrium heme species rather than an on-pathway intermediate.

The 600-fold increase in reaction rate observed in the microcrystals used for the tr-SFX-XFEL experiment compared to large crystals used for EPR spectroscopy is a little unusual. The microcrystals were prepared by vortexing large crystals which shattered them in the *x*, *y*, and *z* directions. While this reduces the crystal size and thickness, the exposed surface area is greatly increased, which means that oxidant is able to diffuse through a small crystal more easily than a large crystal. Additionally, the crystal packing for CYP121 is quite tight, which slows diffusion rate. This effect is clearly visible also in single-crystal absorption spectroscopy measurements, where transition of the ES complex to E upon addition of oxidant is dependent upon crystal size, where larger, thicker crystals take longer (~15 min) to begin the transition compared to smaller, thinner crystals (~6 min). An image of the crystal size difference between microcrystals and large crystals is shown in Figure S14.

The modeling of an H$_2$O$_2$ ligand into the 200-ms tr-SFX-XFELS structure leads to questions regarding the atom source, considering the oxidant used for reaction is peracetic acid which is not observed in the active site. Because PAA is not a pure solution, the other components were screened for their potential role in formation of the intermediate and to determine whether peracetic acid or hydrogen peroxide is the active oxidizer. The peroxides reside in an acidic solution and are mostly protonated. Thus, the impact of pH on the ability of hydrogen peroxide to form the high-spin species was screened from pH 5 – 9 to test the capability of this small molecule to ligate to the heme iron in different protonation ratios. The lack of high-spin species generated at both low and high pH indicates that hydrogen peroxide is not able to easily ligate to the heme iron and initiate catalysis, regardless of its protonation state, which is corroborated by the lower level of product generation compared to peracetic acid. Because peracetic acid is an equilibrium reaction generated by mixing hydrogen peroxide and glacial acetic acid,[58] a 10% hydrogen peroxide oxidant solution was made using this method and stored for a minimum of 24 h at 4°C. In

this instance, a small amount of peracetic acid is expected to be generated, which would form the high-spin heme species. Indeed, this occurs, though at a long time point, likely due to the low concentration of peracetic acid present in solution. At pH 7.4, less than half of the peracetic acid molecules are deprotonated. However, it is likely that these deprotonated molecules ligate to the heme iron more readily and lead to higher levels of product formation which is observed during activity

CYP121 cpd 0   CYP121 O$_2$

Tyrosine hydroxylase   Lactoperoxidase
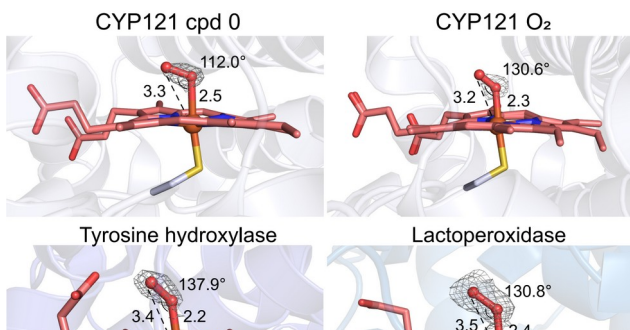
assays when the pH is increased.[20]

It has been demonstrated through computational and model complex studies that the spin state of the ferric-hydroperoxo complex is vital for its reactivity.[59-60] The high-spin state of a ferric hydrogen peroxide adduct due to the weak association and near side-on geometry of the hydrogen peroxide moiety to the iron ion is a novel observation. Comparison of the 2.40 Å heme Fe-S bond length of the 200 ms intermediate to other reported synchrotron X-ray and SFX structures (Table S2) shows that this high-spin state is solely due to the weak association of the near η^2-hydrogen peroxide adduct and comparable iron-sulfur bond distance on the proximal side of the heme as the ES complex structure at 2.37 Å. An early EPR study comparing the high-spin EPR signal of P450s to thiolate-ligated iron porphyrin complexes determined that the presence of the thiolate ligand to the iron ion increased the rhombicity of the high-spin signal compared to complexes with an oxygen or nitrogen axial ligand due to the thiolate pushing the metal ion out of the plane of the porphyrin ring.[61] Nearly a decade later, another study reported an N-ligated peroxo-porphyrin complex with a peroxo ligand presenting a rhombic, high-spin species by EPR though its orientation to the iron ion

could not be fully resolved.[40] In this instance, the high-spin ferric signal is rhombic, with g-values of 9.50, 4.20, and 1.30. More recent studies of N-ligated porphyrin complexes characterized both the side-on and end-on peroxo/hydroperoxo orientations via spectroscopic methods.[44-45] The decay of the side-on to end-on peroxo orientation is observed by protonation of an oxygen atom, tracked by the decay of the g = 4.20 EPR signal to the rhombic low-spin porphyrin complex, corresponding to an end-on ferric-hydroperoxo complex. Thiolate-ligated model complexes used to study the non-heme enzyme superoxide reductase are able to generate a mononuclear ferric-alkylperoxo or hydroperoxo complex upon addition of the corresponding alkylperoxide or O$_2$, with the complexes reported as low-spin by EPR, likely arising from a 6-coordinate end-on species.[49, 62-63] These model complexes give great insight into the spectroscopic characteristics of an unusual side-on ferric-hydroperoxo intermediate structurally observed for the first time in a thiolate heme-based biological system, which determines that the high-spin signal captured in RFQ and single-crystal slurry EPR studies is indeed a weakly-associated hydrogen peroxide cpd 0 intermediate. Additional stopped-flow and RFQ-EPR experiments at low pH using hydrogen peroxide resulted in the intensity of the low-spin signal decreasing, potentially due to an accumulating cpd II species, and no low- to high-spin transition. After a brief period of time, the low-spin signal re-forms.

Comparing this high-spin, ferric-hydroperoxo intermediate with previously reported ferric-peroxo intermediate structures reveals a stark difference in the hydroperoxo binding orientation relative to the heme iron. Those published crystal structures of a ferric- hydroperoxo intermediate directly trapped in an enzyme-mediated catalytic cycle are from histidine-ligated heme-based tyrosine hydroxylase[14] (TyrH) and lactoperoxidase[15] (Figure 5), with all other structures such as chloroperoxidase[2] and myoglobin[10-11] obtained from radiolytic methods (Figure S15). A CYP121 crystal structure bound with O$_2$ in an end-on orientation was also previously reported, which was crystallized in the ferric state and observed due to the synchrotron X-ray beam reduction of the iron center.[47] Comparison of the CYP121 ES complex, enzyme-O$_2$ bound, and cpd 0 intermediate structures is described in Figure S16.

The bond distance range and coordination angles reported for those previously characterized ferric-peroxo intermediates of Fe-O (1.9 – 2.5 Å), O-O (1.3 – 1.6 Å), and Fe-O-O (119 – 138°) are different from the values observed in the CYP121 ferric-hydroperoxo intermediate, which has an Fe-O1 bond length of 2.5 Å, Fe-O2 interaction of 3.3 Å, O-O bond length of 1.4 Å, and an Fe-O-O coordination angle of 111.2° (Table S2). The coordination angle of this intermediate falls well outside the range for reported end-on peroxo intermediates from myoglobin,[10-11] peroxidases,[2] tyrosine hydroxylase,[37] and lactoperoxidase.[15] It sets the chemistry that is performed by this intermediate apart from those intermediates of other reported enzymes. Heme distortion may also play a contributing factor in the more side-on binding orientation of the axial ligand. CYP121 has a much more pronounced heme ruffle

compared to the more planar heme in TyrH and lactoperoxidase (Figure S17). The distal oxygen, which is 3.3 Å from the heme, is 2.9 Å from the phenol oxygen and 3.1 Å from the C3 (ortho to the hydroxy group) of the aromatic ring (Figure S8A), likely a stabilizing factor that allows for the accumulation of the intermediate, ultimately leading to its structural characterization.

The orientation of the hydroperoxo ligand and its proximity to the substrate hydroxy group affects electron movement which dictates the following intermediate in the catalytic cycle and whether it is sufficiently oxidizing to oxidize the substrate. While P450s typically use cpd I as the active oxidant, there is evidence that cpd 0 can drive oxidation reactions,[64] such as in sulfoxidation and *N*-dealkylation by P450 BM3[65] and olefin epoxidation by P450cam.[66] The P450cam mutant T252A demonstrates that disruption of the proton delivery network in the active site forces the enzyme to use an intermediate other than cpd I to oxidize its substrate.[8, 66] Without delivery of a second H^+ to the distal oxygen of the hydroperoxo ligand, the high-valent ferryl species cannot be formed, yet epoxidation of the substrate was detected. This evidence leads to the ferric-hydroperoxo intermediate as the active oxidant for substrate oxidation. Comparison of CYP121 ES complex structure to the active site architecture of 20 representative P450s (Table S3), indicates that the proton delivery network is prevalent in this enzyme family. However, CYP121 is irregular in this respect. The glutamate or aspartate residue is occupied by a non-polar isoleucine and the terminal threonine, which delivers the proton to initiate cpd I formation, is a serine (Figure S18). In conjunction with these residue differences, CYP121 contains an arginine, known to stabilize well-ordered water molecules in the active site and to weakly interact with the tyrosyl moiety of cYY, which resides in an area that is vacant or is generally occupied by a non-polar residue such as valine or leucine in other P450s. This indicates that CYP121 likely does not contain an efficient or effective proton delivery network to facilitate the protonation of cpd 0 for O-O bond cleavage and cpd I formation and, instead, must rely upon its substrate cYY to provide a hydrogen atom.

Similarly, the C-C coupling mechanism mediated by CYP121 potentially uses the cpd 0 intermediate as the active oxidizing species rather than as a prerequisite to prepare for cpd I formation (Scheme 1B). The atypical end-on, which is near-side-on, the orientation of the hydroperoxo ligand positions itself differently from any known heme-based cpd 0 intermediate, orienting the distal oxygen within 3 Å of the substrate hydroxy group, priming it for hydrogen atom abstraction and homolytic cleavage of the O-O bond to form cpd II, which then oxidizes the substrate for a second time for diradical formation and eventual C-C coupling (Figure S19). The formation of cpd II as the second oxidizing species has now been corroborated by using hydrogen peroxide as the oxidant and observing an EPR silent species forming and decaying over a period of one second, along with a concomitant formation and decay of a minor organic radical species. These findings are consistent with the "CYP121 peroxidase" donation and proposed single electron transfer (SET) processes described in an earlier report,[19] and especially the previous finding of activation of the phenolic O-H, rather than a C-H bond, is critical for CYP121 reaction.[20]

CONCLUSION

Since its discovery, CYP121 has been a mechanistic outlier in the P450 catalytic family because it remains predominantly low spin upon substrate binding, setting it apart from most of its superfamily. Therefore, the oxygen activation strategy at early steps, especially the active oxidant, becomes a central focus for revealing CYP121 catalytic mechanism. This cpd 0 intermediate, spectroscopically and structurally observed during the catalytic shunt pathway, reveals a unique binding mode that deviates from the end-on cpd 0 intermediates in other heme enzymes. The mechanism of C-C coupling catalyzed by CYP121 can now be revised to include a ferric-hydroperoxo intermediate, the first of its kind characterized in a thiol-ligated heme-based enzyme, which is of great fundamental importance for the understanding of oxygen activation for noncanonical chemical oxidation mediated by a P450 enzyme.

ASSOCIATED CONTENT

Supporting Information. This material is available free of charge via the Internet at http://pubs.acs.org. Additional data and figures include EPR simulations, structure modeling and refinement, comparison to ferric-peroxo model complexes, and pH-dependent studies, including Figures S1 to S13, Tables S1 to S3, and corresponding references.

AUTHOR INFORMATION

Corresponding Author

Aimin Liu – Department of Chemistry, University of Texas, San Antonio, TX 78249, United States. E-mail: Feradical@utsa.edu
Jan Kern – Molecular Biophysics and Integrated Bioimaging Division, Lawrence Berkeley National Laboratory, Berkeley, CA 94720, United States. E-mail: jfkern@lbl.gov

Authors

Romie C. Nguyen – Department of Chemistry, University of Texas, San Antonio, TX 78249, United States
Ian Davis – Department of Chemistry, University of Texas, San Antonio, TX 78249, United States
Medhanjali Dasgupta – Molecular Biophysics and Integrated Bioimaging Division, Lawrence Berkeley National Laboratory, Berkeley, CA 94720, United States
Yifan Wang – Department of Chemistry, University of Texas, San Antonio, TX 78249, United States
Philipp S. Simon – Molecular Biophysics and Integrated Bioimaging Division, Lawrence Berkeley National Laboratory, Berkeley, CA 94720, United States
Agata Butryn – Diamond Light Source, Harwell Science and Innovation Campus, Didcot, Oxfordshire OX11 0DE, United Kingdom

Research Complex at Harwell, Rutherford Appleton Laboratory, Didcot, Oxfordshire OX11 0FA, United Kingdom

Hiroki Makita – Molecular Biophysics and Integrated Bioimaging Division, Lawrence Berkeley National Laboratory, Berkeley, CA 94720, United States

Isabel Bogacz – Molecular Biophysics and Integrated Bioimaging Division, Lawrence Berkeley National Laboratory, Berkeley, CA 94720, United States

Kednerlin Dornevil – Department of Chemistry, University of Texas, San Antonio, TX 78249, United States

Pierre Aller – Diamond Light Source, Harwell Science and Innovation Campus, Didcot, Oxfordshire OX11 0DE, United Kingdom
Research Complex at Harwell, Rutherford Appleton Laboratory, Didcot, Oxfordshire OX11 0FA, United Kingdom

Asmit Bhowmick – Molecular Biophysics and Integrated Bioimaging Division, Lawrence Berkeley National Laboratory, Berkeley, CA 94720, United States

Ruchira Chatterjee – Molecular Biophysics and Integrated Bioimaging Division, Lawrence Berkeley National Laboratory, Berkeley, CA 94720, United States

In-Sik Kim – Molecular Biophysics and Integrated Bioimaging Division, Lawrence Berkeley National Laboratory, Berkeley, CA 94720, United States

Tiankun Zhou – Diamond Light Source, Harwell Science and Innovation Campus, Didcot, Oxfordshire OX11 0DE, United Kingdom

Derek Mendez – Molecular Biophysics and Integrated Bioimaging Division, Lawrence Berkeley National Laboratory, Berkeley, CA 94720, United States

Daniel Paley – Molecular Biophysics and Integrated Bioimaging Division, Lawrence Berkeley National Laboratory, Berkeley, CA 94720, United States

Franklin Fuller – LCLS, SLAC National Accelerator Laboratory, Menlo Park, CA 94025, United States

Roberto Alonso-Mori – LCLS, SLAC National Accelerator Laboratory, Menlo Park, CA 94025, United States

Alexander Batyuk – LCLS, SLAC National Accelerator Laboratory, Menlo Park, CA 94025, United States

Nicholas K. Sauter – Molecular Biophysics and Integrated Bioimaging Division, Lawrence Berkeley National Laboratory, Berkeley, CA 94720, United States

Aaron S. Brewster – Molecular Biophysics and Integrated Bioimaging Division, Lawrence Berkeley National Laboratory, Berkeley, CA 94720, United States

Allen M. Orville – – Diamond Light Source, Harwell Science and Innovation Campus, Didcot, Oxfordshire OX11 0DE, United Kingdom
Research Complex at Harwell, Rutherford Appleton Laboratory, Didcot, Oxfordshire OX11 0FA, United Kingdom

Vittal K. Yachandra – Molecular Biophysics and Integrated Bioimaging Division, Lawrence Berkeley National Laboratory, Berkeley, CA 94720, United States

Junko Yano – Molecular Biophysics and Integrated Bioimaging Division, Lawrence Berkeley National Laboratory, Berkeley, CA 94720, United States

Notes
The authors declare no competing interests.

REFERENCES

1. Huang, X.; Groves, J. T. Oxygen activation and radical transformations in heme proteins and metalloporphyrins. *Chem. Rev.* **2018**, *118*, 2491-2553.
2. Kühnel, K.; Derat, E.; Terner, J.; Shaik, S.; Schlichting, I. Structure and quantum chemical characterization of chloroperoxidase compound 0, a common reaction intermediate of diverse heme enzymes. *Proc. Natl. Acad. Sci. U.S.A.* **2007**, *104*, 99-104.
3. Rittle, J.; Green, M. T. Cytochrome P450 compound I: capture, characterization, and C-H bond activation kinetics. *Science* **2010**, *330*, 933-937.
4. Jin, S.; Bryson, T. A.; Dawson, J. H. Hydroperoxoferric heme intermediate as a second electrophilic oxidant in cytochrome P450-catalyzed reactions. *J. Biol. Inorg. Chem.* **2004**, *9*, 644-653.
5. Mak, P. J.; Gregory, M. C.; Denisov, I. G.; Sligar, S. G.; Kincaid, J. R. Unveiling the crucial intermediates in androgen production. *Proc. Natl. Acad. Sci. U.S.A.* **2015**, *112*, 15856-15861.
6. Woodward, J. J.; Chang, M. M.; Martin, N. I.; Marletta, M. A. The second step of the nitric oxide synthase reaction: Evidence for ferric-peroxo as the active oxidant. *J. Am. Chem. Soc.* **2009**, *131*, 297-305.

7. Denisov, I. G.; Makris, T. M.; Sligar, S. G. Formation and decay of hydroperoxo-ferric heme complex in horseradish peroxidase studied by cryoradiolysis. *J. Biol. Chem.* **2002**, *277*, 42706-42710.

8. Jin, S.; Makris, T. M.; Bryson, T. A.; Sligar, S. G.; Dawson, J. H. Epoxidation of olefins by hydroperoxo–ferric cytochrome P450. *J. Am. Chem. Soc.* **2003**, *125*, 3406-3407.

9. Denisov, I. G.; Dawson, J. H.; Hager, L. P.; Sligar, S. G. The ferric-hydroperoxo complex of chloroperoxidase. *Biochem. Biophys. Res. Commun.* **2007**, *363*, 954-958.

10. Unno, M.; Chen, H.; Kusama, S.; Shaik, S.; Ikeda-Saito, M. Structural characterization of the fleeting ferric peroxo species in myoglobin: Experiment and theory. *J. Am. Chem. Soc.* **2007**, *129*, 13394-13395.

11. Hersleth, H.; Hsiao, Y.; Ryde, U.; Görbitz, C. H.; Andersson, K. K. The crystal structure of peroxymyoglobin generated through cryoradiolytic reduction of myoglobin compound III during data collection. *Biochem. J.* **2008**, *412*, 257-264.

12. Petrik, I. D.; Davydov, R.; Ross, M.; Zhao, X.; Hoffman, B.; Lu, Y. Spectroscopic and crystallographic evidence for the role of a water-containing H-bond network in oxidase activity of an engineered myoglobin. *J. Am. Chem. Soc.* **2016**, *138*, 1134-1137.

13. Mak, P. J.; Duggal, R.; Denisov, I. G.; Gregory, M. C.; Sligar, S. G.; Kincaid, J. R. Human cytochrome CYP17A1: The structural basis for compromised lyase activity with 17-hydroxyprogesterone. *J. Am. Chem. Soc.* **2018**, *140*, 7324-7331.

14. Wang, Y.; Davis, I.; Shin, I.; Xu, H.; Liu, A. Molecular rationale for partitioning between C-H and C-F bond activation in heme-dependent tyrosine hydroxylase. *J. Am. Chem. Soc.* **2021**, *143*, 4680-4693.

15. Singh, P. K.; Sharma, P.; Bhushan, A.; Kaur, P.; Sharma, S.; Singh, T. P. Structure of a ternary complex of lactoperoxidase with iodide and hydrogen peroxide at 1.77 Å resolution. *J. Inorg. Biochem.* **2021**, *220*, 111461-111469.

16. Belin, P.; Le Du, M. H.; Fielding, A.; Lequin, O.; Jacquet, M.; Charbonnier, J. B.; Lecoq, A.; Thai, R.; Courçon, M.; Masson, C.; Dugave, C.; Genet, R.; Pernodet, J. L.; Gondry, M. Identification and structural basis of the reaction catalyzed by CYP121, an essential cytochrome P450 in *Mycobacterium tuberculosis*. *Proc. Natl. Acad. Sci. U.S.A.* **2009**, *106*, 7426-7431.

17. McLean, K. J.; Carroll, P.; Lewis, D. G.; Dunford, A. J.; Seward, H. E.; Neeli, R.; Cheesman, M. R.; Marsollier, L.; Douglas, P.; Smith, W. E.; Rosenkrands, I.; Cole, S. T.; Leys, D.; Parish, T.; Munro, A. W. Characterization of active site structure in CYP121. A cytochrome P450 essential for viability of *Mycobacterium tuberculosis* H37Rv. *J. Biol. Chem.* **2008**, *283*, 33406-33416.

18. Ortiz de Montellano, P. R. Potential drug targets in the *Mycobacterium tuberculosis* cytochrome P450 system. *J. Biol. Inorg. Chem.* **2018**, *180*, 235-245.

19. Dornevil, K.; Davis, I.; Fielding, A. J.; Terrell, J. R.; Liu, A. Crosslinking of dicyclotyrosine by the cytochrome P450 enzyme CYP121 from *Mycobacterium tuberculosis* proceeds through a catalytic shunt pathway. *J. Biol. Chem.* **2017**, *292*, 13645-13657.

20. Nguyen, R. C.; Yang, Y.; Wang, Y.; Davis, I.; Liu, A. Substrate-assisted hydroxylation and O-demethylation in the peroxidase-like cytochrome P450 enzyme CYP121. *ACS Catal.* **2020**, *10*, 1628-1639.

21. Fielding, A. J.; Dornevil, K.; Ma, L.; Davis, I.; Liu, A. Probing ligand exchange in the P450 enzyme CYP121 from *Mycobacterium tuberculosis*: Dynamic equilibrium of the distal heme ligand as a function of pH and temperature. *J. Am. Chem. Soc.* **2017**, *139*, 17484-17499.

22. Greenspan, F. P.; MacKellar, D. G. Analysis of aliphatic per acids. *Anal. Chem.* **1948**, *20*, 1061-1063.

23. Rajput, S.; McLean, K. J.; Poddar, H.; Selvam, I. R.; Nagalingam, G.; Triccas, J. A.; Levy, C. W.; Munro, A. W.; Hutton, C. A. Structure–activity relationships of cyclo(l-tyrosyl-l-tyrosine) derivatives binding to *Mycobacterium tuberculosis* CYP121: Iodinated analogues promote shift to high-spin adduct. *J. Med. Chem.* **2019**, *62*, 9792-9805.

24. Fuller, F. D.; Gul, S.; Chatterjee, R.; Burgie, E. S.; Young, I. D.; Lebrette, H.; Srinivas, V.; Brewster, A. S.; Michels-Clark, T.; Clinger, J. A.; Andi, B.; Ibrahim, M.; Pastor, E.; de Lichtenberg, C.; Hussein, R.; Pollock, C. J.; Zhang, M.; Stan, C. A.; Kroll, T.; Fransson, T.; Weninger, C.; Kubin, M.; Aller, P.; Lassalle, L.; Bräuer, P.; Miller, M. D.; Amin, M.; Koroidov, S.; Roessler, C. G.; Allaire, M.; Sierra, R. G.; Docker, P. T.; Glownia, J. M.; Nelson, S.; Koglin, J. E.; Zhu, D.; Chollet, M.; Song, S.; Lemke, H.; Liang, M.; Sokaras, D.; Alonso-Mori, R.; Zouni, A.; Messinger, J.; Bergmann, U.; Boal, A. K.; Bollinger, J. M.; Krebs, C.; Högbom, M.; Phillips, G. N.; Vierstra, R. D.; Sauter, N. K.; Orville, A. M.; Kern, J.; Yachandra, V. K.; Yano, J. Drop-on-demand sample delivery for studying biocatalysts in action at X-ray free-electron lasers. *Nature Methods* **2017**, *14*, 443-449.

25. Butryn, A.; Simon, P. S.; Aller, P.; Hinchliffe, P.; Massad, R. N.; Leen, G.; Tooke, C. L.; Bogacz, I.; Kim, I. S.; Bhowmick, A.; Brewster, A. S.; Devenish, N. E.; Brem, J.; Kamps, J.; Lang, P. A.; Rabe, P.; Axford, D.; Beale, J. H.; Davy, B.; Ebrahim, A.; Orlans, J.; Storm, S.; Zhou, T.; Owada, S.; Tanaka, R.; Tono, K.; Evans, G.; Owen, R. L.; Houle, F. A.; Sauter, N. K.; Schofield, C. J.; Spencer, J.; Yachandra, V. K.; Yano, J.; Kern, J. F.; Orville, A. M. An on-demand, drop-on-drop method for studying enzyme catalysis by serial crystallography. *Nat. Commun.* **2021**, *12*, 4461-4468.

26. Campomizzi, C. S.; Ghanatios, G. E.; Estrada, D. F. ¹⁹F-NMR reveals substrate specificity of CYP121A1 in *Mycobacterium tuberculosis*. *J. Biol. Chem.* **2021**, *297*, 101287.

27. Kumar, A.; Campomizzi, C. S.; Jay, N.; Ferguson, S.; Scheffler, E. J.; Lioi, J.; Tu, C.; Qu, J.; Simons, C.; Estrada, D. F. Surface hydrophobics mediate functional dimerization of CYP121A1 of *Mycobacterium tuberculosis*. *Sci. Rep.* **2021**, *11*, Article number 394.

28. Campomizzi, C. S.; Kumar, A.; Uttamrao, P. P.; Stallone, J. J.; Ghanatios, G. E.; Rathinavelan, T.; Estrada, D. F. Active site aromatic residues play a dual role in the substrate interaction and protein structure in functional dimers of CYP121A1 of *Mycobacterium tuberculosis*. *ACS Infect. Dis.* **2023**, *9*, 827-839.

29. Stoll, S.; Schweiger, A. EasySpin, a comprehensive software package for spectral simulation and analysis in EPR. *J. Magn. Reson.* **2006**, *178*, 42-55.

30. Brewster AS; Young ID; Lyubimov A; Bhowmick A; NK, S. Processing serial crystallographic data from XFELs or synchrotrons using the cctbx.xfel GUI. *Computat. Crystallogr. Newsl.* **2019**, *10*, 22-39.

31. Hattne, J.; Echols, N.; Tran, R.; Kern, J.; Gildea, R. J.; Brewster, A. S.; Alonso-Mori, R.; Glöckner, C.; Hellmich, J.; Laksmono, H.; Sierra, R. G.; Lassalle-Kaiser, B.; Lampe, A.; Han, G.; Gul, S.; DiFiore, D.; Milathianaki, D.; Fry, A. R.; Miahnahri, A.; White, W. E.; Schafer, D. W.; Seibert, M. M.; Koglin, J. E.; Sokaras, D.; Weng, T.-C.; Sellberg, J.; Latimer, M. J.; Glatzel, P.; Zwart, P. H.; Grosse-Kunstleve, R. W.; Bogan, M. J.; Messerschmidt, M.; Williams, G. J.; Boutet, S.; Messinger, J.; Zouni, A.; Yano, J.; Bergmann, U.; Yachandra, V. K.; Adams, P. D.; Sauter, N. K. Accurate macromolecular structures using minimal measurements from X-ray free-electron lasers. *Nature Methods* **2014**, *11*, 545-548.

32. Sauter, N. K. XFEL diffraction: Developing processing methods to optimize data quality. *J. Synchrotron Radiat.* **2015**, *22*, 239-248.

33. Sauter, N. K.; Hattne, J.; Brewster, A. S.; Echols, N.; Zwart, P. H.; Adams, P. D. Improved crystal orientation and physical properties from single-shot XFEL stills. *Acta Crystallogr. D Biol. Crystallogr.* **2014**, *70*, 3299-3309.

34. Sauter, N. K.; Hattne, J.; Grosse-Kunstleve, R. W.; Echols, N. New Python-based methods for data processing. *Acta Crystallogr. D Biol. Crystallogr.* **2013**, *69*, 1274-1282.

35. Winter, G.; Waterman, D. G.; Parkhurst, J. M.; Brewster, A. S.; Gildea, R. J.; Gerstel, M.; Fuentes-Montero, L.; Vollmar, M.; Michels-Clark, T.; Young, I. D.; Sauter, N. K.; Evans, G. DIALS: Implementation and evaluation of a new integration package. *Acta Crystallogr. D Struct. Biol.* **2018**, *74*, 85-97.

36. Adams, P. D.; Afonine, P. V.; Bunkoczi, G.; Chen, V. B.; Davis, I. W.; Echols, N.; Headd, J. J.; Hung, L.-W.; Kapral, G. J.; Grosse-Kunstleve, R. W.; McCoy, A. J.; Moriarty, N. W.; Oeffner, R.; Read, R. J.; Richardson, D. C.; Richardson, J. S.; Terwilliger, T. C.; Zwart, P. H. PHENIX: a comprehensive Python-based system for macromolecular structure solution. *Acta Crys. Sec. D* **2010**, *66*, 213-221.

37. Wang, Y.; Liu, K. F.; Yang, Y.; Davis, I.; Liu, A. Observing 3-hydroxyanthranilate-3,4-dioxygenase in action through a crystalline lens. *Proc. Natl. Acad. Sci. U.S.A.* **2020**, *117*, 19720-19730.

38. Schmidt, M. Reaction initiation in enzyme crystals by diffusion of substrate. *Crystals* **2020**, *10*, 116-131.

39. Lang, P. T.; Holton, J. M.; Fraser, J. S.; Alber, T. Protein structural ensembles are revealed by redefining X-ray electron density noise. *Proc. Natl. Acad. Sci. U.S.A.* **2014**, *111*, 237-242.

40. Burstyn, J. N.; Roe, J. A.; Miksztal, A. R.; Shaevitz, B. A.; Lang, G.; Valentine, J. S. Magnetic and spectroscopic characterization of an iron porphyrin peroxide complex. Peroxoferrioctaethylporphyrin (1-). *J. Am. Chem. Soc.* **1988**, *110*, 1382-1388.

41. Chufán, E. E.; Karlin, K. D. An iron–peroxo porphyrin complex: New synthesis and reactivity toward a Cu(II) complex giving a heme–peroxo–copper adduct. *J. Am. Chem. Soc.* **2003**, *125*, 16160-16161.

42. Gallagher, A. T.; Lee, J. Y.; Kathiresan, V.; Anderson, J. S.; Hoffman, B. M.; Harris, T. D. A structurally-characterized peroxomanganese(IV) porphyrin from reversible O_2 binding within a metal–organic framework. *Chem. Sci.* **2018**, *9*, 1596-1603.

43. Gosiewska, S.; van Faassen, E. E.; Permentier, H. P.; Bruins, A. P.; van Koten, G.; Gebbink, R. J. Characterization and alkane oxidation activity of a diastereopure seven-coordinate iron(III) alkylperoxo complex. *Dalton Trans.* **2007**, 3365-3368.

44. Liu, J. G.; Ohta, T.; Yamaguchi, S.; Ogura, T.; Sakamoto, S.; Maeda, Y.; Naruta, Y. Spectroscopic characterization of a hydroperoxo-heme intermediate: conversion of a side-on peroxo to an end-on hydroperoxo complex. *Angew. Chem. Int. Ed. Engl.* **2009**, *48*, 9262-9267.

45. Liu, J. G.; Shimizu, Y.; Ohta, T.; Naruta, Y. i. Formation of an end-on ferric-peroxo intermediate upon one-electron reduction of a ferric superoxo heme. *J. Am. Chem. Soc.* **2010**, *132*, 3672-3673.

46. VanAtta, R. B.; Strouse, C. E.; Hanson, L. K.; Valentine, J. S. Peroxo(tetraphenylporphinato)manganese(III) and chloro(tetraphenylporphinato)manganese(II) anions. Synthesis, crystal structures, and electronic structures. *J. Am. Chem. Soc.* **1987**, *109*, 1425-1434.

47. Leys, D.; Mowat, C. G.; McLean, K. J.; Richmond, A.; Chapman, S. K.; Walkinshaw, M. D.; Munro, A. W. Atomic structure of *Mycobacterium tuberculosis* CYP121 to 1.06 reveals novel features of cytochrome P450 *J. Biol. Chem.* **2003**, *278*, 5141-5147.

48. Melik-Adamyan, W.; Bravo, J.; Carpena, X.; Switala, J.; Maté, M. J.; Fita, I.; Loewen, P. C. Substrate flow in catalases deduced from the crystal structures of active site variants of HPII from *Escherichia coli*. *Proteins* **2001**, *44*, 270-281.

49. Namuswe, F.; Kasper, G. D.; Sarjeant, A. N.; Hayashi, T.; Krest, C. M.; Green, M. T.; Moënne-Loccoz, P.; Goldberg, D. P. Rational tuning of the thiolate donor in model complexes of superoxide reductase: Direct evidence for a *trans* influence in Fe^{III}–OOR complexes. *J. Am. Chem. Soc.* **2008**, *130*, 14189-14200.

50. Davydov, R.; Hoffman, B. M. Active intermediates in heme monooxygenase reactions as revealed by cryoreduction/annealing, EPR/ENDOR studies. *Arch. Biochem. Biophys.* **2011**, *507*, 36-43.

51. Davydov, R.; Makris, T. M.; Kofman, V.; Werst, D. E.; Sligar, S. G.; Hoffman, B. M. Hydroxylation of camphor by reduced oxy-cytochrome P450cam: Mechanistic implications of EPR and ENDOR studies of catalytic intermediates in native and mutant enzymes. *J. Am. Chem. Soc.* **2001**, *123*, 1403-1415.

52. Davydov, R.; Razeghifard, R.; Im, S.-C.; Waskell, L.; Hoffman, B. M. Characterization of the microsomal cytochrome P450 2B4 O2 activation intermediates by cryoreduction and electron paramagnetic resonance. *Biochemistry* **2008**, *47*, 9661-9666.

53. Davydov, R.; Gilep, A. A.; Strushkevich, N. V.; Usanov, S. A.; Hoffman, B. M. Compound I is the reactive intermediate in the first monooxygenation step during conversion of cholesterol to pregnenolone by cytochrome P450scc: EPR/ENDOR/cryoreduction/annealing Studies. *J. Am. Chem. Soc.* **2012**, *134*, 17149-17156.

54. Tsai, R.; Yu, C. A.; Gunsalus, I. C.; Peisach, J.; Blumberg, W.; Orme-Johnson, W. H.; Beinert, H. Spin-state changes in cytochrome P-450cam on binding of specific substrates *Proc. Natl. Acad. Sci. U.S.A.* **1970**, *66*, 1157-1163.

55. Davydov, R.; Im, S.; Shanmugam, M.; Gunderson, W. A.; Pearl, N. M.; Hoffman, B. M.; Waskell, L. Role of the proximal cysteine hydrogen bonding interaction in cytochrome P450 2B4 studied by cryoreduction, electron paramagnetic resonance, and electron–nuclear double resonance spectroscopy. *Biochemistry* **2016**, *55*, 869-883.

56. Davydov, R.; Strushkevich, N.; Smil, D.; Yantsevich, A.; Gilep, A.; Usanov, S.; Hoffman, B. M. Evidence that compound I is the active species in both the hydroxylase and lyase steps by which P450scc converts cholesterol to pregnenolone: EPR/ENDOR/cryoreduction/annealing studies. *Biochemistry* **2015**, *54*, 7089-7097.

57. Davydov, R.; Laryukhin, M.; Ledbetter-Rogers, A.; Sono, M.; Dawson, J. H.; Hoffman, B. M. Electron paramagnetic resonance and electron-nuclear double resonance studies of the reactions of cryogenerated hydroperoxoferric–hemoprotein intermediates. *Biochemistry* **2014**, *53*, 4894-4903.

58. Zhao, X.; Ting, Z.; Yu-Jie, Z.; De-Hua, L. Preparation of peracetic acid from acetic acid and hydrogen peroxide: Experimentation and modeling. *Chinese J. Proc. Eng.* **2008**, *8*, 35-41.

59. Dey, A.; Solomon, E. I. Density functional theory calculations on Fe–O and O–O cleavage of ferric hydroperoxide species: Role of axial ligand and spin state. *Inorg. Chim. Acta* **2010**, *363*, 2762-2767.

60. Zaragoza, J. T.; Goldberg, D. P., Chapter 1 Dioxygen binding and activation mediated by transition metal porphyrinoid complexes. In *Dioxygen-dependent Heme Enzymes*, The Royal Society of Chemistry: 2019; pp 1-36.

61. Sato, M.; Kon, H.; Kumaki, K.; Nebert, D. W. Comparative EPR study on high-spin ferric porphine complexes and cytochrome P450 having rhombic character. *Biochem. Biophys. Acta* **1977**, *498*, 403-421.

62. Jiang, Y.; Telser, J.; Goldberg, D. P. Evidence for the formation of a mononuclear ferric–hydroperoxo complex via the reaction of dioxygen with an (N$_4$S(thiolate))iron(II) complex. *Chem. Comm.* **2009**, 6828-6830.

63. Shearer, J.; Scarrow, R. C.; Kovacs, J. A. Synthetic models for the cysteinate-ligated non-heme iron enzyme superoxide reductase: Observation and structural characterization by XAS of an FeIII–OOH intermediate. *J. Am. Chem. Soc.* **2002**, *124*, 11709-11717.

64. Vaz, A. D.; Pernecky, S. J.; Raner, G. M.; Coon, M. J. Peroxo-iron and oxenoid-iron species as alternative oxygenating agents in cytochrome P450-catalyzed reactions: Switching by threonine-302 to alanine mutagenesis of cytochrome P450 2B4. *Proc. Natl. Acad. Sci. U.S.A.* **1996**, *93*, 4644-4648.

65. Volz, T. J.; Rock, D. A.; Jones, J. P. Evidence for two different active oxygen species in cytochrome P450 BM3 mediated sulfoxidation and N-dealkylation reactions. *J. Am. Chem. Soc.* **2002**, *124*, 9724-9725.

66. Vaz, A. D.; McGinnity, D. F.; Coon, M. J. Epoxidation of olefins by cytochrome P450: Evidence from site-specific mutagenesis for hydroperoxo-iron as an electrophilic oxidant. *Proc. Natl. Acad. Sci. U.S.A.* **1998**, *95*, 3555-3560.

Table of Contents artwork